Modeling of Flow-Induced Crystallization of Particle-Filled Polymers

Wook Ryol Hwang,[†] Gerrit W. M. Peters,[‡] Martien A. Hulsen,[‡] and Han E. H. Meijer*[,‡]

School of Mechanical and Aerospace Engineering, Research Center for Aircraft Parts Technology (ReCAPT), Gyeongsang National University, Jinju, 660-701, South Korea, and Materials Technology, Eindhoven University of Technology, P.O. Box 513, 5600MB, Eindhoven, The Netherlands

Received May 30, 2006; Revised Manuscript Received September 25, 2006

ABSTRACT: We present a study on flow-induced crystallization of polymers filled with rigid particles. The numerical simulations reveal the interplay between filler particles, the polymer melt, flow, and flow-induced crystallization. Both crystallization kinetics and the resulting crystal orientation are affected, and they are crucial for the material properties that are created during flow. In the analysis of the problem, first a direct 2D numerical simulation technique for viscoelastic particle suspensions is applied to determine the local molecular conformation during the flow. Subsequently, we use this conformation as the driving force for flow-induced crystallization. Local anisotropic crystalline structures are formed due to high molecular orientation, especially near the particles. Because of the presence of the same particles, regions of the melt are shielded from the flow, and therefore, hardly any effect of the flow is seen in these regions. Both coupled and decoupled simulations were performed. In the last approximation the flow problem is solved using a generalized Newtonian viscous fluid model, and the velocity gradients obtained are plugged into a viscoelastic constitutive model that provides the molecular conformation. It is found that the decoupled method gives incorrect results, especially with respect to the molecular and crystalline structure orientation.

I. Introduction

The pioneering work of the Du Pont−MIT group (Argon and Cohen from MIT) on toughness improvement of different semicrystalline polymers using hard fillers rather than soft rubbers[1−9] inspired a number of research groups to try to reproduce these intriguing results that for the first time allowed the combination of an impact strength improvement with an increase (rather than decrease) in Young's modulus. One of those groups, Schrauwen et al.,[10] measured the impact toughness of injection molded samples of a system extensively investigated by DuPont/MIT: high-density polyethylene (HDPE) filled with calcium carbonate ($CaCO_3$) particles. They compared the results with samples prepared via compression molding. Reproducing the DuPont−MIT results proved to be not easy. It was found that the results could be quantitatively reproduced if, and only if, exactly the same mold geometry was used. (At DuPont a tensile test bar mold was used to make an impact specimen by cutting the bar after molding in two parts: one from the gate side and the other from the end side.) Schrauwen et al. confirmed that the impact toughness significantly increased with imposed shear rate, especially for particle volume fractions around 15%. The Argon and Cohen group basically tried to explain the improved properties by reaching the threshold for percolating transcrystalline layers that grow on the surface of the particles. Schrauwen et al., however, emphasized the more dominant influence of flow. In the injection-molded samples flow influence was already demonstrated by the DuPont/MIT group as expressed in different properties near the injection gate compared to at the end of the test samples. In the compression-molded samples of the same material (with almost no flow) very little toughness enhancement was observed in Schrauwen et al.[10] This is already indicative for the possibly dominating influence of the flow history. By using a square test plate, rather than the rectangular test bar that only produces test samples in flow direction, also the direction perpendicular to flow could be tested.[10] As expected in accordance with the compression test samples, no toughness improvement was found in the samples perpendicular to flow direction. Further studies, by using X-ray scattering over the thickness of the samples, revealed the existence of flow-induced crystalline structures, parallel to the flow direction, not only near the wall—the high shear region where one would expect orientation—but also in the core region where velocity gradients are absent. The presence of the particles was thought to be responsible for this peculiar phenomena, since flowing particles locally increase the velocity gradients and moreover introduce elongational flow in between the particles as they separate. In this way, an increase of the influence of flow on the crystallization kinetics and crystal orientation can be expected. Slow relaxation of molecular orientation causes the flow history, as experienced in the extrusion unit and in the runners of the injection unit, to be still partly present in the melt once it enters the mold cavity. This partly explains the orientation effects observed in the core of the products. A different approach to study the problem was performed by the TU Eindhoven−MIT group (Boyce and Parks from MIT): the multilevel modeling approach, developed in Eindhoven, was extended to try to explain the behavior of particle-filled semicrystalline polymers.[11−18] These studies reveal that the anisotropic crystal plasticity induced due to supposed transcrystalline layers percolating through the structure is not sufficient to explain the enhanced ductility and toughness found. For this, indeed an overall flow-induced crystal orientation in the direction of the flow proved to be needed. Recently, Corté and Leibler[19−22] demonstrated, by using elaborate TEM analyses, that the existence of transcrystalline layers in particle-filled systems analogous to those used in the previous studies mentioned could not be confirmed and that only an overall flow-induced crystal orientation was found in these injection-molded particle-filled heterogeneous systems. Even more convincing were the experiments where they, in a confined way, remelted

[†] Gyeongsang National University.
[‡] Eindhoven University of Technology.
* Corresponding author: Tel +31-402472851; Fax +31-402447355; e-mail h.e.h.meijer@tue.nl.

10.1021/ma061205g CCC: $33.50
Published on Web 10/28/2006

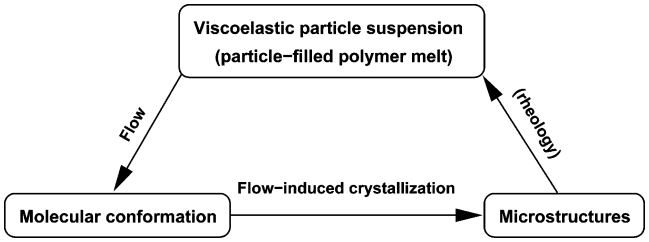

Figure 1. Flow-induced crystallization in particle-filled polymers is influenced by the molecular conformation of polymers determined by the flow.

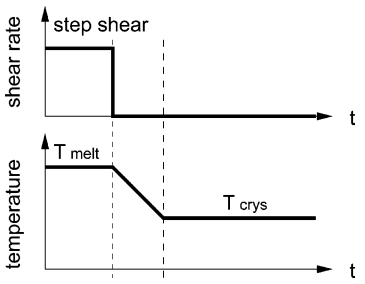

Figure 2. The prototype two-step model problem.

and recrystallized the samples in the absence of flow. The improved toughness earlier found directly after molding was lost.

From these experiments and simulations we can conclude that the impact improvement found in injection-molded particle-filled semicrystalline polymers (either with hard fillers but also with soft, rubbery, fillers) is, at least partly, due to the anisotropic crystal structures caused by flow-induced crystallization. Flow-induced crystallization in polymers correlates with the stresses that occur during viscoelastic flow much more than with the macroscopic strain or the strain rate.[23,25−27] This implies that the molecular conformation, i.e., chain orientation and chain stretch, is the governing factor controlling flow-induced crystallization.[23,25,26] Moreover, it is especially the high end tail of the molecular weight distribution, with the largest relaxation time, that produces the oriented fiberlike (shish) structure.[28] Since particles disturb the flow field, a significant effect of the presence of particles on flow-induced crystallization is expected.

This is the topic of the present work, where we present a numerical model for flow-induced crystallization in particle-filled semicrystalline polymers. The model enables us to study the effect of the presence of rigid particles in a viscoelastic shear flow on the molecular conformation and thus on anisotropic flow-induced crystallization. This is a complex task since it involves (i) nonlinear viscoelastic material behavior, (ii) hydrodynamic interaction between multiple particles, and (iii) nonisothermal phase changes. Moreover, these three complexities are strongly coupled. To keep the computations manageable, we introduce a simplified model problem that attains the key features of the whole process but still can be solved with current computational methods at affordable costs.

The way we define the problem is shown in Figure 1. The crystallization problem is separated from the flow problem, and to simplify the problem, the circle in Figure 1 is not closed but instead a model problem is defined composed of the following two-step procedure (Figure 2): *P1: Flow problem,* the application of simple shear flow for a certain time at a temperature above the melting temperature. *P2: Crystallization problem,* cessation of the flow, i.e., stress relaxation, and simultaneously cooling to the crystallization temperature. During this stage the evolution of flow-induced crystallization is determined.

The temperature in the first step is chosen sufficiently high such that nucleation and growth are absent. We obtain the polymer stress, i.e., the molecular conformation in this step. Next, the molecular conformation is used as the driving force for the flow-induced crystallization. Notice that this simple two-step procedure is also a prototype model for an injection-molding process: a shear-dominant flow during filling and cooling after cessation of the flow.

To solve the first step, we use a direct numerical simulation (DNS) technique for a viscoelastic particle suspension in simple shear flow,[29,30] and we compare fully coupled viscoelastic flow simulation results with decoupled analyses. In the second step, we solve the kinetics of flow-induced crystallization, following Zuidema et al.,[23] with the molecular conformation from the first step as the initial driving force. Crystallization kinetics is, in general, described by two separate sets of equations: one for quiescent crystallization and one for flow-induced crystallization that are additive in nature. Here, however, we are interested in the resulting flow-induced structures and will only use that corresponding set of equations. Moreover, the crystallization temperature is deliberately chosen to be high in order to focus on the development of the flow-induced crystallization and to emphasize the effects of flow on crystal anisotropy. At a high temperature, crystallization is slow and the kinetics of quiescent crystallization can be neglected. In real injection molding, both crystallization processes are active, and the large undercooling that occurs makes quiescent crystallization dominant. In addition, the flow-induced structure makes the samples anisotropic, and that is why we constructed the schedule according to Figure 2.

For complex flows, such as occur in injection molding, it is in general not possible to perform fully coupled simulations (3D, compressible, nonisothermal, nonlinear viscoelastic, free surfaces), and especially the high Weissenberg numbers involved are problematic. A standard way to get around this last problem is to solve the flow kinematics using a generalized Newtonian viscous model and use the resulting kinematics in a nonlinear viscoelastic model to compute the transient stresses. It has been shown that this approach works well for shear dominated flows (see Douven et al.[31]), which is the case for injection molding. We will test the validity of this important simplification for the filled polymeric systems considered here.

II. Modeling and Computational Methods

A. Flow of Filled Polymer Melts: The Coupled Approach. Filled polymer melts can be modeled as a viscoelastic particle suspension consisting of a large number of freely suspended non-Brownian hard particles for which inertia effects can be neglected, for both the matrix fluid and particles. The best method, until now, to solve this problem is a direct numerical simulation technique as was recently developed for particle suspensions in a sliding biperiodic frame: a well-defined biperiodic computational domain in simple shear flow.[29,30] By introducing a sliding biperiodic frame, a particulate flow in a unit domain represents the flow of the suspension, and one can minimize finite-sized domain effects such as wall interactions. Figure 3 shows the sliding biperiodic frames and a possible particle configuration in a single frame at a certain instance (for details refer to ref 29).

The numerical methods used in this study to simulate the flow of viscoelastic particle suspensions are essentially the same as those presented in ref 30, except for the constitutive equation for describing polymer melt rheology. Here we will use the Leonov model[32] which gives a good description of the nonlinear

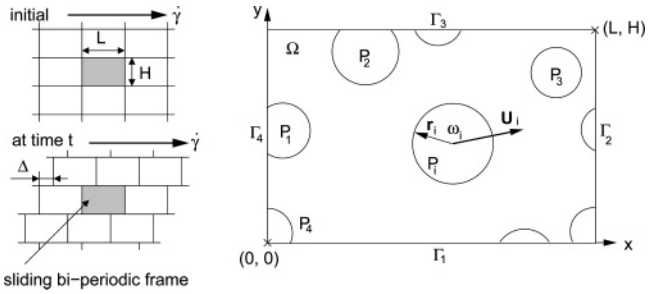

Figure 3. Sliding biperiodic frames in a simple shear flow (left). A sliding biperiodic frame is the computational domain and a possible particle configuration inside the domain is indicated (right).

behavior of a polymeric fluid, especially in shear dominated flows. The advantage is that the model only requires linear input data.

The set of equations governing the fluid domain is given by the equations of continuity, the momentum balance, and the constitutive equation:

$$\nabla\cdot\mathbf{u} = 0, \quad \nabla\cdot\boldsymbol{\sigma} = 0, \quad \boldsymbol{\sigma} = -p\mathbf{I} + 2\eta_s\mathbf{D} + \boldsymbol{\tau}_p \qquad (1)$$

where $\mathbf{u}$, p, $\mathbf{D}$, $\boldsymbol{\sigma}$, $\mathbf{I}$, $\boldsymbol{\tau}_p$, and η_s are the velocity, the pressure, the rate-of-deformation tensor, the total stress, the identity tensor, the polymeric contribution to the extra stress tensor, and the solvent viscosity, respectively. The viscoelastic polymer stress $\boldsymbol{\tau}_p$ is further specified by the Leonov model for incompressible planar deformation:

$$\dot{\boldsymbol{\tau}}_p + \frac{1}{\lambda}\boldsymbol{\tau}_p + \frac{1}{2G\lambda}\boldsymbol{\tau}_p\cdot\boldsymbol{\tau}_p = 2G\mathbf{D} \qquad (2)$$

where λ is the relaxation time, G is the shear modulus, and the symbol $\cdot$ in eq 2 denotes the upper-convected time derivative, defined as

$$\dot{\boldsymbol{\tau}}_p \equiv \frac{\partial\boldsymbol{\tau}_p}{\partial t} + \mathbf{u}\cdot\nabla\boldsymbol{\tau}_p - (\nabla\mathbf{u})^T\cdot\boldsymbol{\tau}_p - \boldsymbol{\tau}_p\cdot\nabla\mathbf{u}$$

The domain occupied by the particles is expressed by the rigid-ring description.[29,30] The description is based on the fictitious domain method, where objects moving through a continuum fluid (rotors, screws, impellers, heart valves, etc.) are described by—for the fluid—additional constraints (like zero normal velocities) positioned on the surface of the object that move with the objects. The strength of this elegant method is the lack of need for continuous remeshing. In this work, particles are considered as rigid rings, which are filled with the same fluid as present in the fluid domain. The rigid-body motion of a particle, which is determined by torque-free and force-free conditions on the particle boundary, is imposed only on the ring, not on the interior of the particle. In fact, the rigid ring behaves exactly the same as the rigid particle, whenever inertia is negligible.

To derive the weak form, we implement the following in the finite element method used: (i) mortar elements to get smooth solutions for velocity, pressure, and the viscoelastic stress across the boundaries of the sliding biperiodic frame; (ii) the fictitious domain method, similar to that of Glowinski et al.,[35] for the implicit solution of the particle−fluid interaction; (iii) discrete elastic−viscous stress splitting (DEVSS) with discontinuous Galerkin (DG) for a stable solution of the viscoelastic flow problem.

The above combination of numerical methods was verified to give accurate and stable solutions of viscoelastic particle suspension flows, if incorporated with appropriate discretization of variables and suitable choice of the time-stepping method. We use regular quadrilateral elements for the discretization of the whole computational domain, including the interior of the particles with continuous biquadratic interpolation for the velocity $\mathbf{u}$, discontinuous linear interpolation for the pressure p, continuous bilinear interpolation for the viscous polymer stress, which comes from the DEVSS formulation, and discontinuous bilinear interpolation for the polymer stress $\boldsymbol{\tau}_p$. For the time-stepping method, we used the second-order Adams−Bashforth method for the integration of the viscoelastic stress evolution equation and of the Lagrangian particle movement. Details of implementation techniques can be found in ref 30.

B. Flow of Filled Polymer Melts: The Decoupled Approach. In the decoupled approach, first the velocity field is computed using a generalized Newtonian viscosity model. Next the viscoelastic stresses are computed using this velocity field. The Carreau−Yasuda model is employed including a Newtonian solvent viscosity, η_s, to make direct comparison with the coupled simulation possible:

$$\eta_{cy}(II_{2\mathbf{D}}) = \eta_s + \frac{\eta_0}{(1 + (\lambda_{cy}|\,II_{2\mathbf{D}}|^{1/2})^a)^{(1-n)/a}} \qquad (3)$$

The numerical method used for solving the decoupled problem is almost the same as for the Newtonian particle suspension problem.[29] The only difference is the additional Picard-type iteration that is required to deal with the nonlinearity of the shear-thinning viscosity. With this method, a separate routine is needed to integrate the viscoelastic stress evolution equation (eq 2), using the velocity field at each time step. For the stabilization of the integration of the convection term in eq 2, we use the weak form with the discontinuous Galerkin (DG) method. Again, the same values of λ and G of the single representative mode as in the coupled flow simulation are used.

C. Flow-Induced Crystallization during Relaxation. After cessation of the flow, the recoverable strain $\mathbf{B}_e$ is determined from the viscoelastic stress $\boldsymbol{\tau}_p$ according to

$$\mathbf{B}_e = \frac{\boldsymbol{\tau}_p}{G_l} + \mathbf{I} \qquad (4)$$

This is done for the longest relaxation mode only (denoted by the subscript l) since this mode governs the flow-induced nucleation. The second invariant of the deviatoric part of $\mathbf{B}_e$, denoted by $J_2(\mathbf{B}_e^d)$, is taken as the driving force for the flow-induced crystallization.

$$J_2(\mathbf{B}_e^d) = \frac{1}{2}\mathbf{B}_e^d:\mathbf{B}_e^d, \quad \mathbf{B}_e^d = \mathbf{B}_e - \frac{1}{2}\mathrm{tr}(\mathbf{B}_e)\mathbf{I} \qquad (5)$$

$J_2(\mathbf{B}_e^d)$ represents a combined measure for the molecular orientation and stretch.[34] The evolution of the tensor $\mathbf{B}_e$ can also be described by the Leonov model:

$$\dot{\mathbf{B}}_e + \frac{1}{2\lambda_l(T)}(\mathbf{B}_e\cdot\mathbf{B}_e - \mathbf{I}) = \mathbf{0} \qquad (6)$$

Using eq 4, it is easy to show that eq 6 is equivalent to eq 2. The subscript l denotes the largest relaxation time mode. $\dot{\mathbf{B}}_e$ is just $\partial\mathbf{B}_e/\partial t$ for the no flow condition. For this reason, we used a pointwise computation in integrating eq 6 together with a second-order Adams−Bashforth method in time. While integrat-

ing eq 6, the temperature dependence of the relaxation time λ_l is taken into account during cooling.

In describing flow-induced crystallization kinetics, we use the S_{J2} model,[23] which is an improvement of the original model of Eder and Janeschitz-Kriegl[27] in that the recoverable strain is used for the driving force of the flow-induced crystallization rather than the shear rate. The S_{J2} model has the same structure as the Schneider's rate equation.[33] The mean number of flow-induced oriented structures (shish-kebabs) and their mean length, surface, and volume are calculated according to

$$\dot{\psi}_3 + \frac{\psi_3}{\tau_n} = 8\pi J_2(\mathbf{B}_e^d) g'_n, \quad (\psi_3 = 8\pi \tilde{N}_f), \quad \text{"rate"}$$

$$\dot{\psi}_2 + \frac{\psi_2}{\tau_l} = J_2(\mathbf{B}_e^d)\frac{g'_l}{g'_n}\psi_3, \quad (\psi_2 = 8\pi L_{\text{total}}), \quad \text{"length"}$$

$$\dot{\psi}_1 = \tilde{G}\psi_2, \quad (\psi_1 = S_{\text{total}}), \quad \text{"surface"}$$

$$\dot{\psi}_0 = \tilde{G}\psi_1, \quad (\psi_0 = V_{\text{total}}), \quad \text{"volume"}$$

$$\psi_0 = -\ln(1 - \xi_f), \quad \text{"space filling"} \tag{7}$$

The parameters g'_n and g'_l describe the sensitivity of the number and length of flow-induced nuclei on $J_2(\mathbf{B}_e^d)$, respectively. $\tilde{G}$ denotes the temperature-dependent growth rate. The parameters τ_n and τ_l are the characteristic times of the relaxation behavior of the flow-induced nuclei and length, respectively. The quantity ξ_f is the degree of the space filling due to flow-induced crystallization only. The impingement of the cylindrical structures is expressed by an Avrami-type model, and the morphological structure is described per unit volume by the total volume of shish-kebabs V_{total}, their total surface S_{total}, the sum of their length L_{total}, and the number of flow-induced nuclei $\tilde{N}_f$.

The flow-induced crystallization kinetics equation (eq 7) is solved using a pointwise integration with the second-order Adams−Bashforth method. Initially, ψ_i ($i = 1, 2, 3, 4$) is set to zero. Next, at every time step, for given $\mathbf{B}_e^n$, ψ_i^n, T^n, and λ^n, we compute ψ_i^{n+1}, λ^{n+1}, and $\mathbf{B}_e^{n+1}$ ($i = 1, 2, 3, 4$) explicitly, by using eqs 6 and 7.

III. Material Parameters

The data set for isotactic Polypropylene Daplen KS10 (Borealis, MW = 235 kg/mol), a polymer extensively studied in our group, is used here.[23,24,27] The (four mode) linear viscoelastic data (G_i,λ_i) for $T = 200$ °C, the flow temperature, are listed in Table 1. The first mode, with the shortest relaxation time, is taken into account as a Newtonian solvent, i.e., $\eta_s = G_1\lambda_1$, and the remaining three modes are cast into a single representative mode in order to avoid excessive Weissenberg numbers that potentially appear using a spectrum of relaxation times (where always one large relaxation time could be present). To do so, we introduce the viscosity-averaged relaxation time as the single characteristic relaxation time λ:

$$\lambda = \frac{\sum_{i=2}^{4}\eta_i\lambda_i}{\sum_{i=2}^{4}\lambda_i} = \frac{\sum_{i=2}^{4}G_i\lambda_i^2}{\sum_{i=2}^{4}G_i\lambda_i} \tag{8}$$

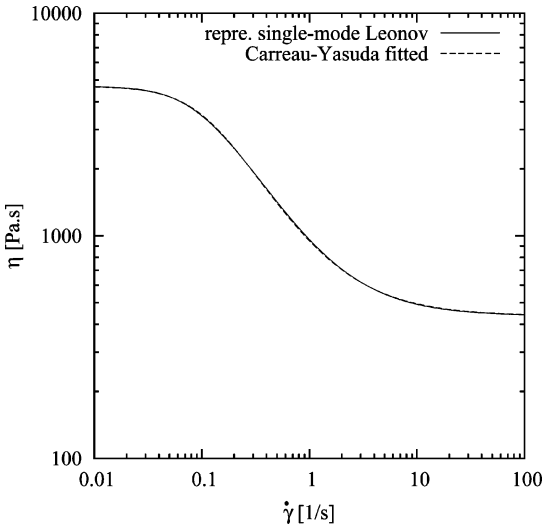

Figure 4. Comparison of the viscosity of the fitted Carreau−Yasuda model and the Leonov model with the single representative mode.

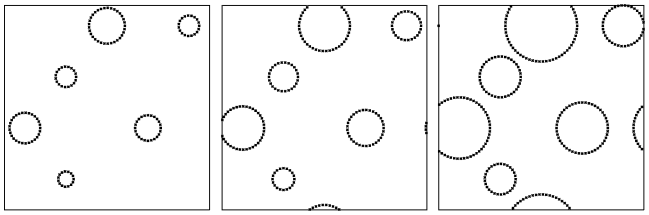

Figure 5. Initial configurations of the particles in the slding biperiodic frame for three sets of test problems: the solid area fraction $\phi = 0.075$, 0.15, and 0.30 from the left.

Table 1. Linear Viscoelastic Data of Daplen KS10 at $T = 200$ °C (Refs 23, 24, and 27)

mode i	G_i [Pa]	λ_i [s]
1	5.547×10^4	8.0×10^{-3}
2	1.210×10^4	1.144×10^{-1}
3	1.208×10^3	1.568×10^{-0}
4	3.3×10^1	2.974×10^1

Table 2. Materials Properties of Daplen KS10 Related to the Flow-Induced Crystallization Behavior (Refs 23, 24, and 27)

growth rate $\tilde{G}$		
c_G [K^{-2}]	G_{ref} [m/s]	T^G_{cref} [°C]
2.3×10^{-3}	5.012×10^{-6}	90
S_{J2} parameters		
g'_n [m^{-3} s^{-1}]	g'_l [m/s]	τ_l and τ_n [s]
2.017×10^{11}	1.429×10^{-1}	∞

and the corresponding characteristic shear modulus G is defined as

$$G = \frac{\sum_{i=2}^{4}G_i\lambda_i}{\lambda} \tag{9}$$

The values of η_s, λ, and G are 436.56 Pa·s, 7.5862 s, and 561.51 Pa, respectively. The polymer viscosity $\eta_p = G\lambda$ is then 4259.8 Pa·s.

The same solvent viscosity η_s ($= G_1\lambda_1$) is used in the Carreau−Yasuda model in eq 3. The remaining four parameters η_0, λ_{cy}, a, and n in eq 3 were determined to give the best fit for the viscosity curve with the single representative mode data of the Leonov model in the coupled flow simulation. Figure 4

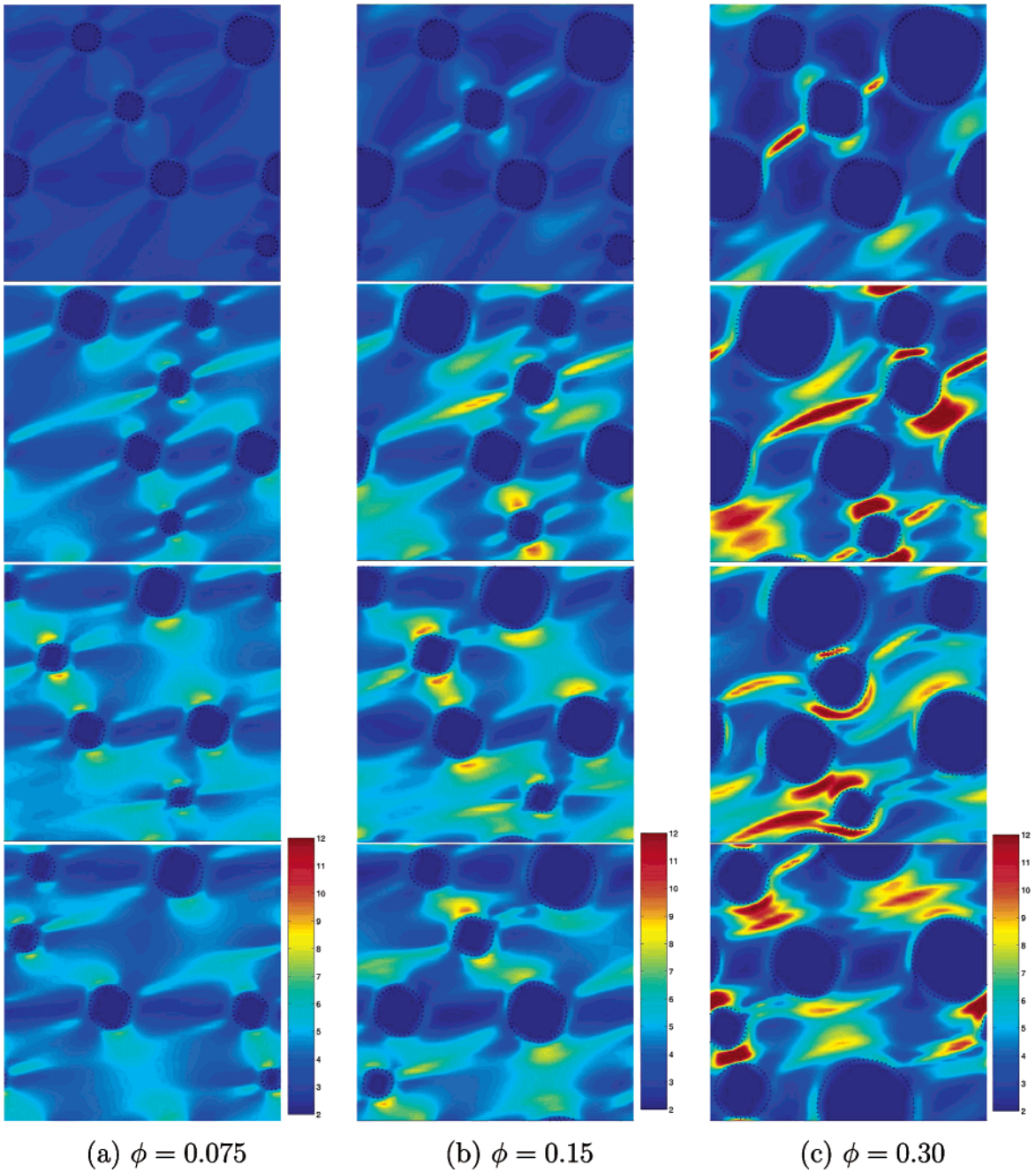

Figure 6. Distribution of the trace of the recoverable strain tensor $\mathbf{B}_e$ at different times under the flow using a fully coupled viscoelastic simulation: from the top to the bottom, $t = 2(0.26\lambda)$, 4 (0.53λ), 10 (1.32λ), and 20 (2.64λ) s, respectively. Flow direction is horizontal

shows the viscosity curve for the Leonov model and for the fitted Carreau−Yasuda model. The values of η_0, λ_{cy}, a, and n are 4260 Pa·s, 9.2 s, 1.77, and 0.05, respectively.

The change of the relaxation time λ_l during cooling is described using the WLF equation.

$$\log a_T = -\frac{c_1(T - T_{ref})}{c_2 + (T - T_{ref})} \tag{10}$$

in which the parameter values $c_1 = 1.0 \times 10^1$ and $c_2 = 1.0 \times 10^3$ K at $T_{ref} = 200$ °C. In addition, we take the fourth viscoelastic mode, the longest relaxation mode, for λ_l and G_l used in eqs 4 and 6.

When solving the flow-induced crystallization kinetics equation (eq 7), the relaxation times for nuclei τ_n and for shish τ_l have been set to infinite, since the associated relaxation occurs only through remelting which is not the case in our simplified model problem. We also neglect the effect of flow-induced nuclei on the increase of the relaxation time or of the viscosity. (We do not close the sysem as described in Figure 1 but only use the simplified problem sketched in Figure 2.) The time scale of the isothermal crystallization experiments at the high temperature chosen can typically be $O(10^4$ s) for quiescent crystallization and mild flow conditions (Wi < 1). For strong flow conditions (Wi ≫ 1) this reduces to $O(10-10^3$ s). However, we cannot deal (yet) with flows having such a high Weissenberg number. Therefore, we limit ourselves to Wi = $O(1)$ flows and, to keep the time scale in the simulations within reasonable proportions, we scale the characteristic time in the kinetic equations such that the effect of the invariant $J_2(\mathbf{B}_e^d)$ is increased by a factor of 10^2. The results obtained are still correct in a qualitative sense.

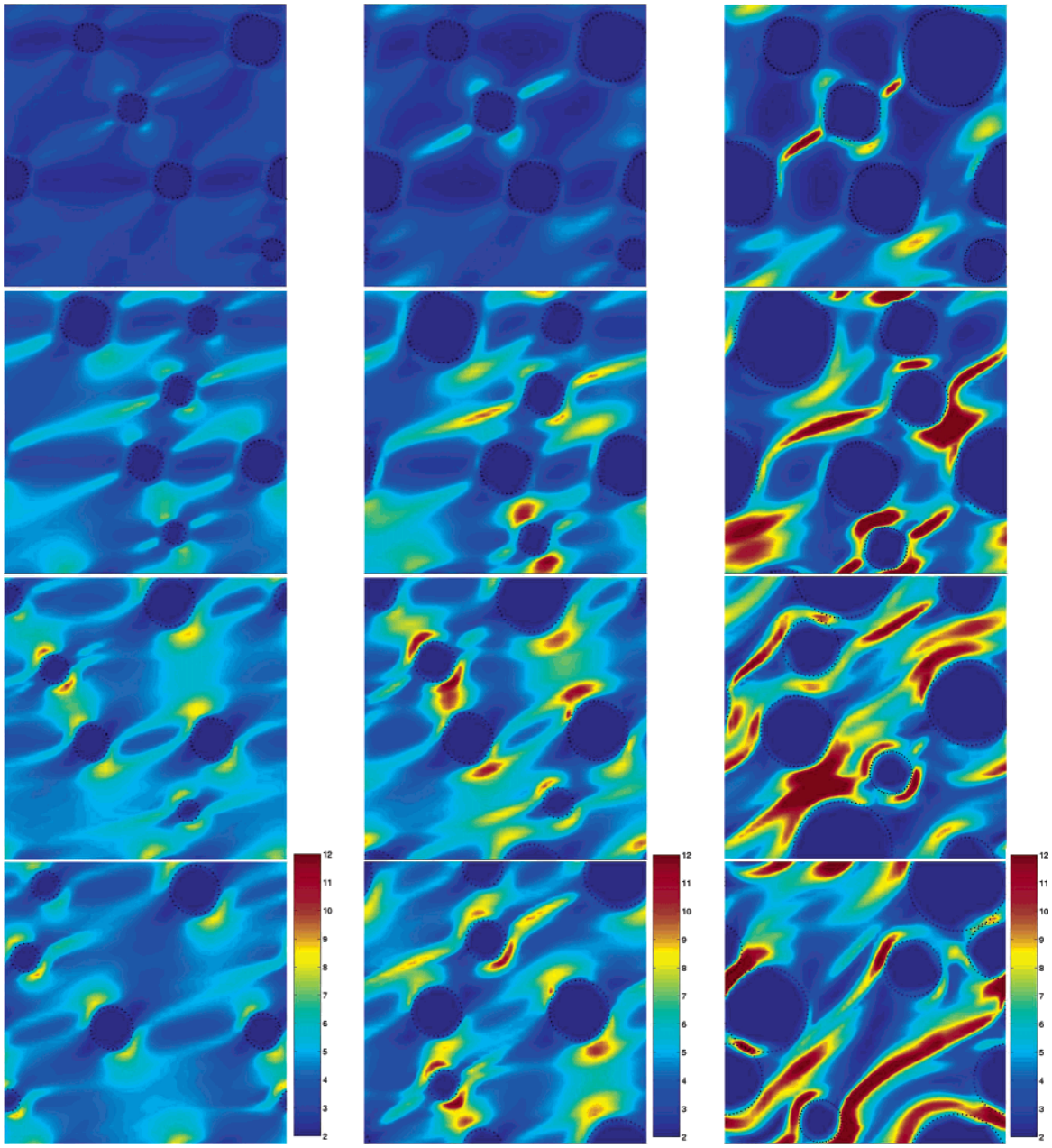

Figure 7. As Figure 6, now for decoupled simulations.

Finally, the growth rate $\tilde{G}$ in the S_{J2} model (eq 7) is described by the function of the temperature as well:

$$\tilde{G}(T) = G_{\text{ref}} \exp(-c_G(T - T^{G}_{\text{cref}})^2) \qquad (11)$$

The values of G_{ref}, c_G, and T^{G}_{cref} are listed in Table 2 along with the parameters of the S_{J2} model.

IV. Results

Three sets of six particle problems with different solid area fraction: $\phi = 7.5\%$, 15%, and 30% were tested. The initial particle configuration is given in Figure 5. For all simulations a shear rate $\dot{\gamma} = 0.5\ \text{s}^{-1}$ was imposed, the corresponding Weissenberg number, $\text{Wi} = \lambda\dot{\gamma}$, was 3.8, and the shear time was 20 s. The domain size, 1×1, was discretized by a 50×50 fluid mesh. For the coupled viscoelastic flow simulations the time step was 0.0005 s; for the decoupled simulations it was 0.01 s for solving the velocity field and 0.001 s for solving the viscoelastic stresses. Computing the crystallization kinetics equation with the relaxation of the tensor $\mathbf{B}_e$ was done with a the time step of 0.5 s. The temperature during flow was set to 200 °C, and the temperature during crystallization was 136 °C. The rate of cooling for the temperature transition was −100 °C/s.

Figure 6 shows, for the coupled viscoelastic flow simulations, the distribution of the trace of the tensor $\mathbf{B}_e$ for each six-particle problem at $t = 2$ (0.26λ), 4 (0.53λ), 10 (1.32λ), and 20 (2.64λ) s. It is observed that the high molecular stretch region (colored red) increases with the solid fraction ϕ. There seem to be two mechanisms generating high molecular stretch. One is the high elongational stretch generated between passing and separating particles that has been reported also in our previous work.[30] The elongational stretch is a typical phenomenon in concentrated viscoelastic suspensions; it is not observed in Newtonian

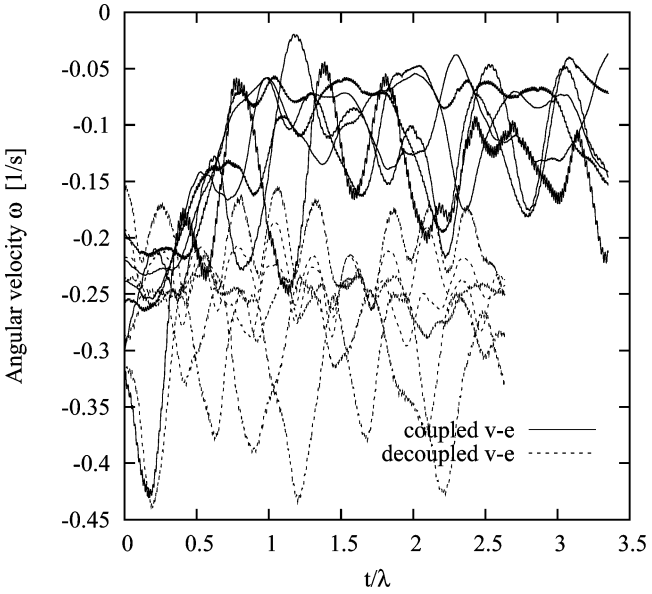

Figure 8. Comparison of the particle angular velocities between the coupled viscoelastic simulation and the decoupled viscoelastic simulations for the $\phi = 15\%$ case.

suspensions. Even if two particles are separated over a distance larger than several times the particle diameter, the stretch is still developing. The other high stretch region is found near the top and the bottom of particles, especially when two particles are in near vicinity. Both mechanisms for molecular stretch become more dominant when increasing the solid area fraction. This could explain the existence of a critical interparticle distance for impact improvement experimentally found in filled (either with hard fillers of with soft fillers) semicrystalline polymers.

Figure 7 shows again the distribution of the trace of the tensor $\mathbf{B}_e$, but now for the decoupled flow simulation. Similar results to the previous ones in Figure 6 are observed: the stretch generated by the separating particles and the stretch appearing near the top and the bottom of the particle. Moreover, the effect of the particle fraction on the level and the size of the high stretch region is also the same as for the coupled simulation. However, there is also an evident difference between the two results: the orientation in the molecular stretch between separating particles is, in the coupled simulations, much more aligned in the shear direction than for the decoupled simulations. Also, the level of stretch is found to be lower for the coupled simulations. To interpret the difference, we present in Figure 8 the transient particle angular velocities for both the coupled and the decoupled simulations for the case of $\phi = 15\%$. (Though not presented here, the translational velocity of the particle does not differ much for the two cases.) In a Newtonian fluid, for a shear rate $\dot{\gamma} = 0.5\ s^{-1}$, an isolated particle rotates at an angular velocity $\omega = -0.25\ s^{-1}$. For the decoupled simulation using the Carreau−Yasuda model, the particle angular velocity fluctuates around this value. However, for the Leonov fluid, particles rotate much slower although the shear-dependent viscosity is the same for both fluids (Figure 4). Similar results were presented for an Oldroyd-B fluid where the particle angular rotation was reduced with increasing elasticity.[30] The larger particle rotation in the (generalized) Newtonian fluid is considered to cause the increased level in molecular stretch and the tilted orientation of stretch in the decoupled simulations; particles act as stirrers. One could also state that in viscoelastic flows the free rotation of particles is hindered. Thus, in shear flow they more or less rotationless slide over each other, giving rise to molecular orientations in the shear direction. And that is the direction in which the crystal orientation is experimentally found, e.g., by Schrauwen et al.[10] and by Corté and Leibler.[19−22]

Notice that for both cases also low stretch regions exist in between particles. In the case of the coupled simulations, the low stretch region appears between particles in the shear direction, a region shielded by two particles in line with the shear direction. It is observed that the size of the low stretch regions increase with the solid fraction ϕ. Similarly, there are low stretch regions between particles in the decoupled simulation, but now tilted 45° with respect to the shear direction. This is also related to the higher angular velocity of particles in the decoupled simulations.

From the numerical simulations it can be concluded that the presence of particles in polymer melts does produce not only highly oriented molecular stretch but, at the same time, regions of low stretch; even lower than the stretch found in a pure viscoelastic flow without particles. We call this the shielding effect of the particles and its effect becomes more evident when more or bigger particles are added. Both effects enhance crystal anisotropy (see below), and also the shielding effect could be of relevance for the critical interparticle distance experimentally found.

The highly nonhomogeneous molecular conformation in a particle-filled polymer directly affects flow-induced crystallization. Figure 9 shows the spatial distribution of the degree of space filling ξ_f due to flow-induced crystallization at different instances after stopping the flow for the coupled flow simulations. The quantity ξ_f increases in time for all three cases ($\phi =$ 7.5%, 15%, and 30%), and crystalline structures are created in those regions where highly stretched molecules are present. At the same time, in the shielded regions no crystalline structures are developed, even after 8000 s at the high, constant, crystallization temperature used. In the early stage of flow-induced crystallization, the amount of particles is found to be a critical factor to initiate nucleation and crystallization. However, in the final stage, one can observe that for $\phi = 30\%$, the highest filler fraction, the crystallized regions are less well developed than for the other cases.

Figure 10 gives the spatial distribution of ξ_f at the same instances as previously depicted in Figure 9 for $\phi = 7.5\%$, 15%, and 30%, now for the decoupled simulations. Similar phenomena as with the coupled simulations are observed: flow-induced space filling, ξ_f, increases in time, especially where high molecular stretch is present, and in the early stage of crystallization, it increases with the solid fraction ϕ. Also, the shielded regions, where crystallinity hardly develops, are seen even after 8000 s, and again, the size of such regions increases with ϕ. However, there is an evident difference when comparing with the coupled results: the orientation of the crystalline structures is now tilted 45° from the shear direction, whereas in the coupled simulations the orientation was more aligned in shear direction. It is clear that decoupled simulation techniques do not provide reliable results in the case of freely suspended particles in a viscoelastic medium.

Figure 11 shows the domain-averaged flow-induced degree of space filling ξ_f for $\phi = 0$ (no particle), 7.5%, 15%, and 30% (in taking the average, we excluded the area occupied by the particles). The results show that, in the early stage of crystallization, the averaged flow-induced crystallinity increases faster in the filled systems when compared to the unfilled system. In this stage, the rate of increase of the flow-induced averaged crystallinity is proportional to the particle fraction. However, in the later stages ($t \approx 5000$ s) the unfilled system reaches the

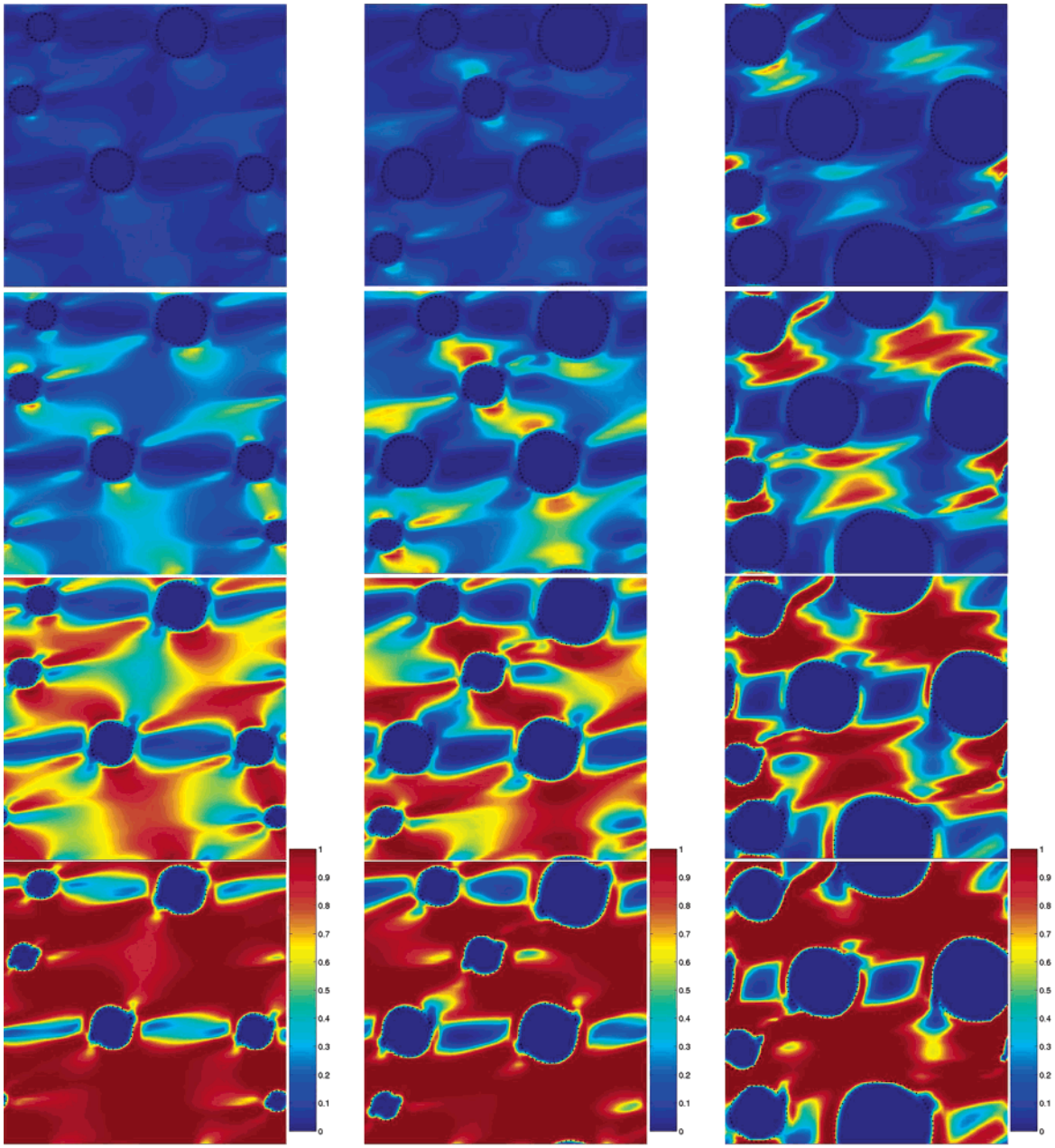

Figure 9. Distribution of the degree of the space filling ξ_f due to flow-induced crystallization at four different times after cessation of the flow using the tensor $\mathbf{B}_e$ from the coupled viscoelastic flow simulation: from the top to the bottom, $t = 1000$, 2000, 4000, and 8000 s. Flow direction is horizontal.

fully crystallized state ($\xi_f = 1$) earlier than the filled systems. In fact, the rate of increase of the averaged crystallinity is reciprocal to the solid fraction in the late stage of flow-induced crystallization.

This phenomenon can be understood from the nonhomogeneous viscoelastic stress distribution in the filled system. The faster increase of the averaged ξ_f in the early phase originates from highly oriented and localized molecular stretch between separating particles and around particles. However, the slower increase in the averaged ξ_f for the filled system in the late stage is due to the low level of molecular stretch in the shielded regions. The molecular stretch in those regions is lower than in that of the unfilled system which is distributed uniformly in the domain. The effect of the amount of filled particles can be understood also in this way.

V. Conclusions

In this study, we performed numerical simulations to understand flow effects on flow-induced crystallization phenomena in particle-filled polymer melts. Flow-induced crystallization is correlated with molecular conformation, more specific with the orientation and stretch of the molecules with the longest relaxation time. To enhance the effects of flow, a typical experimental procedure for the characterization of flow-induced crystallization was mimicked by introducing a simple two-step numerical procedure: (i) a flow problem of viscoelastic particle suspensions under simple shear and (ii) a flow-induced crystallization problem during cooling without flow. By taking a sufficiently high temperature for the flow problem, we could neglect the nucleation and crystallization during the first step. Such a simplification is required since the complete process

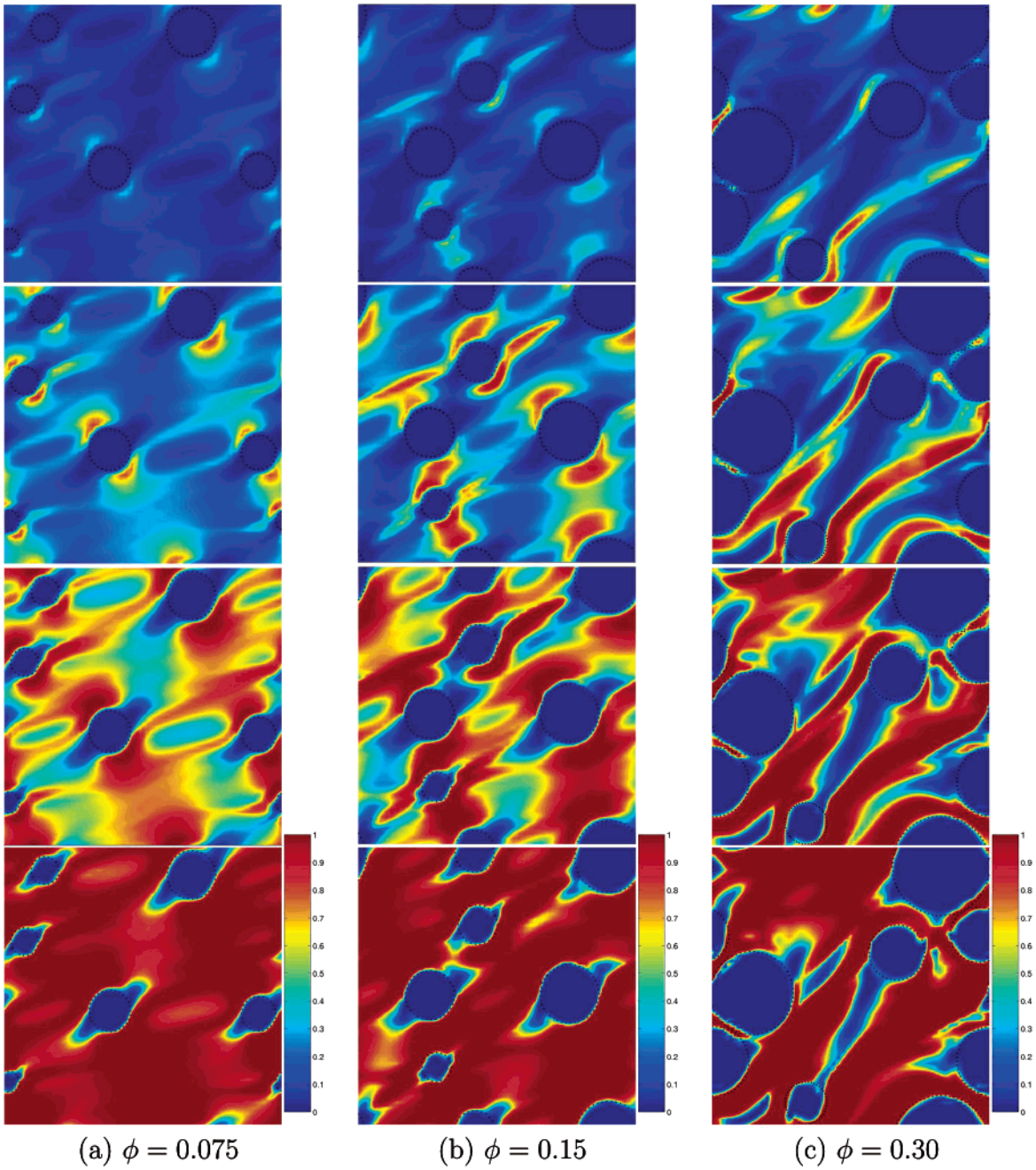

Figure 10. As Figure 9, now for the decoupled simulations.

involves complex transient nonisothermal fluid rheology, hydrodynamic interactions, and phase changes at the same time. This cannot be captured by the existing models yet.

Simple shear flow of viscoelastic particle suspensions has been solved with a direct numerical simulation method developed by the authors using the sliding biperiodic domain concept. The recoverable strain, taken from the flow simulations at a certain instance, is used as the input for the second problem of flow-induced crystallization during stress relaxation. The kinetics are described by the S_{J2} model that uses the second invariant of the deviatoric part of the recoverable strain $J_2(\mathbf{B}_e^d)$ as the driving force for the flow-induced crystallization. To understand the viscoelastic flow effect clearly, we also presented the comparative decoupled flow simulation results together with the associated flow-induced crystallization. In the decoupled simulations, we used the Carreau−Yasuda model, for which the parameters were determined to give the same shear-dependent viscosity as for the Leonov model that was used in the fully coupled simulations.

A highly oriented and nonhomogeneous elongational stretch of molecules was found between two separating particles and near the top and the bottom of particles that are close. Also, low-shear regions with an average molecular stretch lower than in the pure viscoelastic fluid for the same shear flow were found between particles. We called this the shielding effect of particles. Both effects depend on the number of particles present and could help to explain the existence of a critical interparticle distance as experimentally found, since crystal anisotropy is thought to be the cause of this. Two main differences between the coupled and decoupled viscoelastic flow analyses are observed: (i) the molecular orientation of and the position and shape of the low sheared regions and (ii) the level of the stretch. Both orientations were found to be more aligned in the shear direction in the coupled simulations when compared to the decoupled simula-

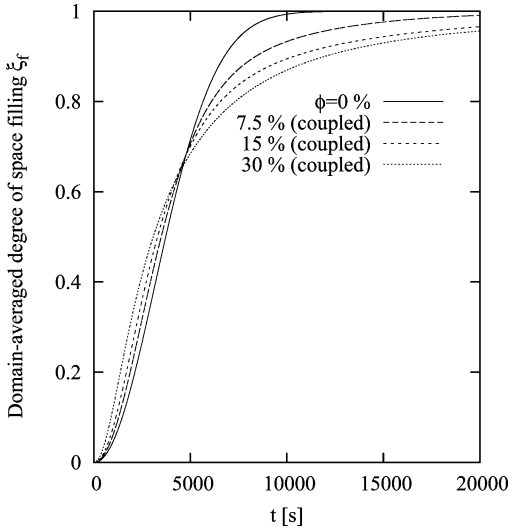

Figure 11. Evolution of the domain-averaged degree of space filling ξ_f in time for different solid fraction from the coupled simulation (comparable with Figure 9).

tions. Also, the level of the molecular stretch was found to be lower. These differences were interpreted by presenting the angular velocity of particles. The particle rotation in the viscoelastic fluid is much smaller (roughly 3 times) than that in the Carreau−Yasuda fluid. This results in a more rotationless sliding of particles in shear flow, resulting in molecular orientation in shear direction. From the subsequent analyses of flow-induced crystallization it was found that the domain-averaged crystallinity in the filled systems grows faster than in the early stage of the crystallization process, but later it is slower in reaching the fully crystallized state compared to the unfilled systems. We interpreted this by emphasizing the heterogeneous distribution of the molecular stretch, as resulted from flow simulations: regions of the high molecular stretch are responsible for the fast growth of the crystallinity in the early phase in filled system, and the low stretch region due to the shielding effect of particles is the source of delayed increase in the overall crystallinity for the filled system. An important conclusion of this study is that, in accordance with the differences in orientation of the molecular stretch, also the orientation of the resulting flow-induced crystalline structures is found to be aligned much more in the shear direction in the case of the coupled simulations compared to the uncoupled simulations. This compares well with experiments; see e.g. Schrauwen et al.[10] and Corté and Leibler.[19−22] Thus, only fully coupled simulations are able to correctly predict the structure formation and the resulting anisotropy in particle-filled polymer systems. This is bad news since it complicates the analyses of these processes considerable. However, it is also good news, now for those specialized in developing stable numerical solutions of high Weissenberg flows where recently a breakthrough was reported.[36−38] Remember, the Weissenberg numbers in polymer processing in general, and in injection molding especially, are rather high.

Acknowledgment. The authors are indebted to the Dutch Polymer Institute (Research Project 161) and the Korea Research Foundation (Grant KRF-2005-005-J09902) for financial support.

References and Notes

(1) Muratoglu, O. K.; Argon, A. S.; Cohen, R. E.; Weinberg, M. *Polymer* **1995**, *36*, 921−930.
(2) Muratoglu, O. K.; Argon, A. S.; Cohen, R. E. *Polymer* **1995**, *36*, 2143−2152.
(3) Muratoglu, O. K.; Argon, A. S.; Cohen, R. E.; Weinberg, M. *Polymer* **1995**, *36*, 4771−4786.
(4) Bartczak, Z.; Galeski, A.; Argon, A. S.; Cohen, R. E. *Polymer* **1996**, *37*, 2113−2123.
(5) Bartczak, Z.; Argon, A. S.; Cohen, R. E.; Kowalewski, T. *Polymer* **1999**, *40*, 2367−2380.
(6) Bartczak, Z.; Argon, A. S.; Cohen, R. E.; Weinberg, M. *Polymer* **1999**, *40*, 2331−2346.
(7) Bartczak, Z.; Argon, A. S.; Cohen, R. E.; Weinberg, M. *Polymer* **1999**, *40*, 2347−2365.
(8) Wilbrink, M. W. L.; Argon, A. S.; Cohen, R. E.; Weinberg, M. *Polymer* **2001**, *42*, 10155−10180.
(9) Thio, Y. S.; Argon, A. S.; Cohen, R. E.; Weinberg, M. *Polymer* **2002**, *43*, 3661−3674.
(10) Schrauwen, B. A. G.; Govaert, L. E.; Peters, G. W. M.; Meijer, H. E. H. *Macromol. Symp.* **2002**, *185*, 89−102.
(11) van Dommelen, J. A. W.; Schrauwen, B. A. G.; van Breemen, L. C. A.; Govaert, L. E. *J. Polym. Sci., Polym. Phys. Ed.* **2004**, *42*, 2983−2994.
(12) van Dommelen, J. A. W.; Brekelmans, W. A. M.; Baaijens, F. P. T. *Comput. Mater. Sci.* **2003**, *27*, 480−492.
(13) van Dommelen, J. A. W.; Parks, D. M.; Boyce, M. C.; Brekelmans, W. A. M.; Baaijens, F. P. T. *Polymer* **2003**, *44*, 6089−6101.
(14) van Dommelen, J. A. W.; Brekelmans, W. A. M.; Baaijens, F. P. T. *Mech. Mater.* **2003**, *35*, 845−863.
(15) van Dommelen, J. A. W.; Parks, D. M.; Boyce, M. C.; Brekelmans, W. A. M.; Baaijens, F. P. T. *J. Mech. Phys. Solids* **2003**, *51*, 519−541.
(16) van Dommelen, J. A. W.; Brekelmans, W. A. M.; Baaijens, F. P. T. *J. Mater. Sci.* **2003**, *38*, 4393−4405.
(17) van Dommelen, J. A. W.; Brekelmans, W. A. M.; Baaijens, F. P. T. *Int. J. Numer. Methods Eng.* **2000**, *48*, 1311−1330.
(18) van Dommelen, J. A. W.; Meijer, H. E. H. In *Mechanical Properties of Polymers Based on Nanostructure and Morphology*; Michlet, G. H., Balta-Calleja, F. J., Eds.; CRC Press: Boca Raton, FL, 1999; pp 317−378.
(19) Corté, L.; Beaume, F.; Leibler, L. *Polymer* **2005**, *46*, 2748−2757.
(20) Corté, L.; Leibler, L. *Polymer* **2005**, *46*, 6360−6368.
(21) Corté, L.; Leibler, L. *Macromolecules* **2006**, *39*, 2445−2448.
(22) Corté, L. Renforcement de polymères semicrystallins, Ph.D. Thesis, Universite Pierre et Marie Curie, 2006.
(23) Zuidema, H.; Peters, G. W. M.; Meijer, H. E. H. *Macromol. Theory Simul.* **2001**, *10*, 447−460.
(24) Swartjes, F. H. M.; Peters, G. W. M.; Rastogi, S.; Meijer, H. E. H. *Int. Polym. Proc.* **2003**, *18*, 53−66.
(25) Peters, G. W. M.; Swartjes, F. H. M.; Meijer, H. E. H. *Macromol. Symp.* **2002**, *185*, 277−292.
(26) Peters, G. W. M. In *Polymer Crystallization*; Sommer, J. U., Reiter, G., Eds.; Springer: Berlin, 2003; pp 312−324.
(27) Eder, G.; Janeschitz-Kriegl, H. In *Materials Science and Technology*; Meijer, H. E. H., Ed.; Verlag Chemie: Berlin, 1997; Vol. 18, pp 269−342.
(28) Seki, M.; Thurman, D. W.; Oberhauser, J. P.; Kornfield, J. A. *Macromolecules* **2002**, *35*, 2583−2594.
(29) Hwang, W. R.; Hulsen, M. A.; Meijer, H. E. H. *J. Comput. Phys.* **2004**, *194*, 742−772.
(30) Hwang, W. R.; Hulsen, M. A.; Meijer, H. E. H. *J. Non-Newtonian Fluid Mech.* **2004**, *121*, 15−33.
(31) Douven, L. F. A.; Baaijens, F. P. T.; Meijer, H. E. H. *Prog. Polym. Sci.* **1995**, *20*, 403−457.
(32) Leonov, A. I. *Rheol. Acta* **1976**, *15*, 85−98.
(33) Schneider, W.; Köppl, A.; Berger, J. *Int. Polym. Proc.* **1988**, *2*, 151−154.
(34) Larson, R. G. *Constitutive Equations for Polymer Melts and Solutions*; Butterworths: London, 1988.
(35) Glowinski, R.; Pan, T.-W.; Hesla, T. I.; Joseph, D. D. *Int. J. Multiphase Flow* **1999**, *25*, 755−794.
(36) Fattal, R.; Kupferman, R. *J. Non-Newtonian Fluid Mech.* **2004**, *124*, 281−285.
(37) Hulsen, M. A.; Fattal, R.; Kupferman, R. *J. Non-Newtonian Fluid Mech.* **2005**, *127*, 27−39.
(38) Fattal, R.; Kupferman, R. *J. Non-Newtonian Fluid Mech.* **2005**, *126*, 23−27.

MA061205G